Natural Resources Canada | Ressources naturelles Canada

GEOLOGICAL SURVEY OF CANADA
OPEN FILE 8016

Chinkeh Formation, northeastern British Columbia: detrital zircon geochronology sample descriptions, methodology and data tables

W. Matthews, M. McMechan, F. Ferri, and B. Guest

2016

Canada

GEOLOGICAL SURVEY OF CANADA
OPEN FILE 8016

Chinkeh Formation, northeastern British Columbia: detrital zircon geochronology sample descriptions, methodology and data tables

W. Matthews[1], M. McMechan[2], F. Ferri[3], and B. Guest[1]

[1] Centre for Pure and Applied Tectonics and Thermochronology, Department of Geosciences, University of Calgary, 2500 University Drive N.W., Calgary, Alberta
[2] Geological Survey of Canada, 3303 – 33rd Street N.W., Calgary, Alberta
[3] Petroleum Geoscience Section, Tenure and Geoscience Branch, Ministry of Natural Gas Development, Victoria, British Columbia

2016

doi:10.4095/298756

This publication is available for free download through GEOSCAN (http://geoscan.nrcan.gc.ca/).

Recommended citation
Matthews, W., McMechan, M., Ferri, F., and Guest, B., 2016. Chinkeh Formation, northeastern British Columbia: detrital zircon geochronology sample descriptions, methodology and data tables; Geological Survey of Canada, Open File 8016, 1 .zip file. doi:10.4095/298756

Publications in this series have not been edited; they are released as submitted by the author.

TABLE OF CONTENTS

ABSTRACT

Sandstone, shale and conglomerate of the Chinkeh Formation occur at the base of the Cretaceous section in the Liard Basin of northeastern British Columbia, southeastern Yukon and southwestern Northwest Territories. The age of this unit and the degree of western provenance has been a source of debate. This report provides sample information, detrital zircon methodology and the complete filtered data tables for the suite of samples from the Chinkeh Formation. These data document an Albian to latest Aptian age for the formation and a dominant recycled Ellesmerian provenance.

INTRODUCTION

The Liard Basin, a sub-basin of the Western Canada Sedimentary Basin, is characterized by anomalously thick Upper Paleozoic and mid-Cretaceous strata. The Basin, bounded on the east by the deep-seated Bovie Lake Structure (Figure 1), contains up to 5 km of Phanerozoic strata. The sub-Cretaceous unconformity forms the most important stratigraphic break within the basin as it progressively truncates strata to the north and east. Sandstone, shale and conglomerate of the Chinkeh Formation form an irregular unit at the base of the Cretaceous succession. Biostratigraphic studies of the Chinkeh Formation have suggested ages ranging from Hauterivian to Aptian to entirely Albian (Braman and Hills, 1977; Leckie et al., 1991; Jowett, 2004). Four samples of the Chinkeh formation were collected as part of a larger study examining the detrital zircon provenance of the Liard Basin (McMechan et al., 2015). The data presented here form the analytical basis of the detrital zircon geochronology presented in McMechan et al. (2016) that documents an Albian to possibly latest Aptian age for the Chinkeh Formation in the eastern Liard Basin. The data also document a dominant recycled Ellesmerian provenance (McMechan et al., 2015). Tombstone information for each sample and the detrital zircon methodology are presented in the following sections. The detrital zircon results are presented in the accompanying Excel File.

CHINKEH FORMATION SAMPLE INFORMATION

Alaska Highway Mile 375 (Tetsa River Lodge) Locality

Two samples were collected by M. McMechan from the 3.85 m thick Chinkeh Formation at the Mile 375 Alaska Highway outcrop of Stott (1982, Figure 1) located across the highway from Tetsa River Lodge (Figure 1) in NTS 094K (0428145E, 6502088N NAD83, zone 10).

Field No. 14MBB015D01; GSC Curation No. C-591527; DZ lab number: UK013

Lithology: orange brown weathering, medium grey, fine to very fine grained, slightly calcareous sandstone with local chert pebbles and a few larger sandstone clasts at base. In outcrop this forms the lower part of a 0 to 0.95 m thick channel fill at the base of the Chinkeh Formation (Figure 2).

Field No. 14MBB015C01; GSC Curation No. C-591523; DZ lab number: UK014

Lithology: rusty brown weathering, light grey, very fine grained, sharp based and topped sandstone. In outcrop this is interbedded with dark grey silty shale (Figure 2) and occurs near the top of a shaling upward sequence.

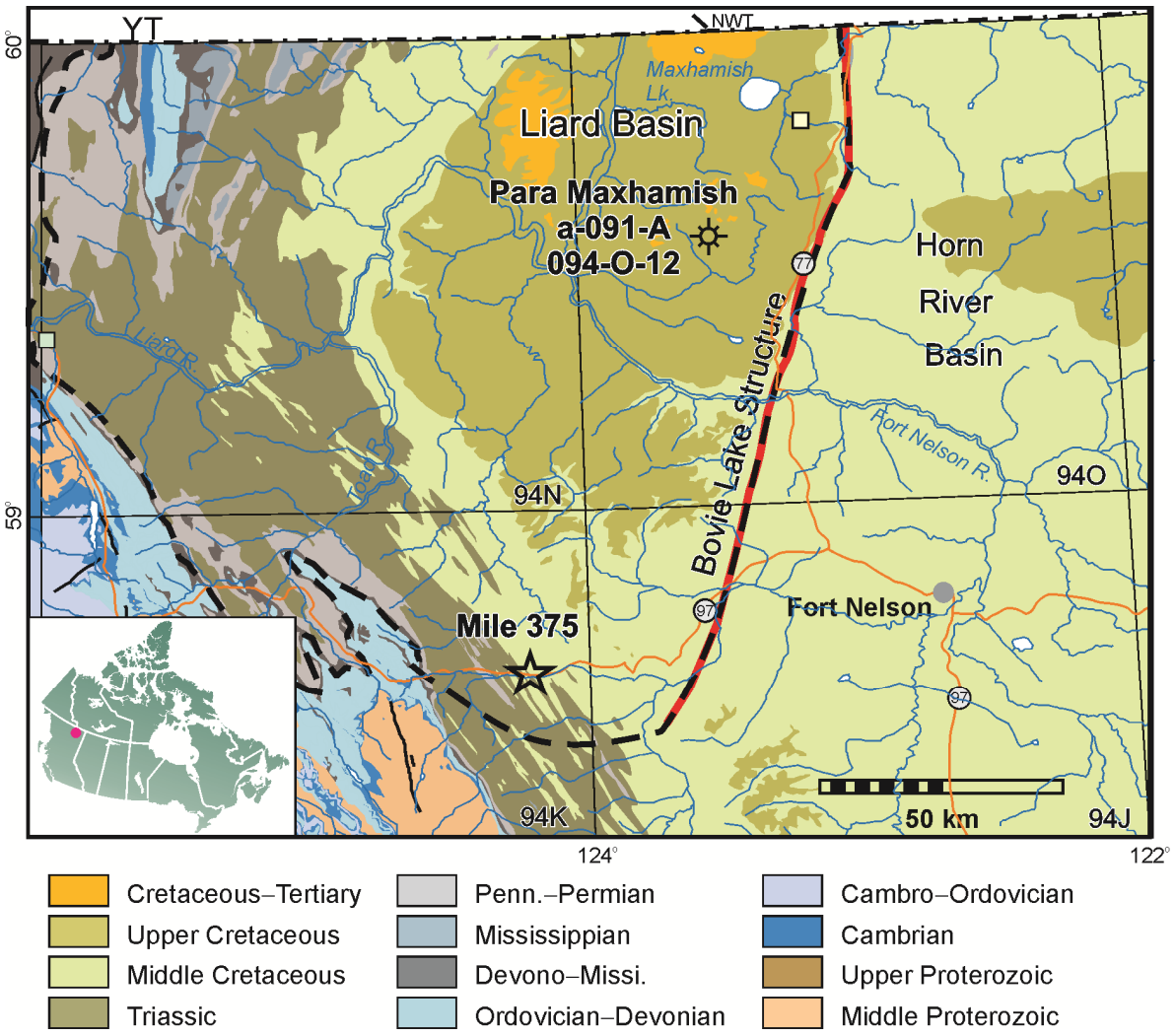

Figure 1. Location of Chinkeh Formation detrital zircon samples, Liard Basin, British Columbia.

Para Maxhamish a-091-A/094-O-12 core

Three samples were collected by M. McMechan from a core through the Chinkeh Formation in the Para Maxhamish a-091-A/094-O-12 well located in the eastern part of the Liard Basin (Figures 1 and 3). Because of restrictions in the permitted sample size it was planned that the upper 2 samples would be combined to form a detrital zircon sample for the Chinkeh Formation. The lower sample was thought to be from the Triassic Liard Formation and a large sample size was permitted. Detrital zircon geochronology results required a mid-Cretaceous age and that the sample was from the Chinkeh Formation.

Field No. WA10748 1779.725-1779.75m; GSC Curation No. C-591328; and Field No. WA1078 1780.35-1780.44m; GSC Curation No. C-591329; DZ lab number: UK014

Lithology: laminated, glauconitic sandstone. Collected from between 1779.725 to 1779.75 m and 1780.35 to 1780.44 m driller's depth.

Field No. WA10748_1788.1-1788.2m; GSC Curation No. C-591330; DZ lab number: UK016

Lithology: beige, bioturbated and laminated more and less silty sandstone. Collected from between 1788.1 to 1788.2 m driller's depth.

Figure 2. Sample locations from the Chinkeh Formation section, Mile 375, Tetsa River Lodge locality on the Alaska Highway, northeastern British Columbia.

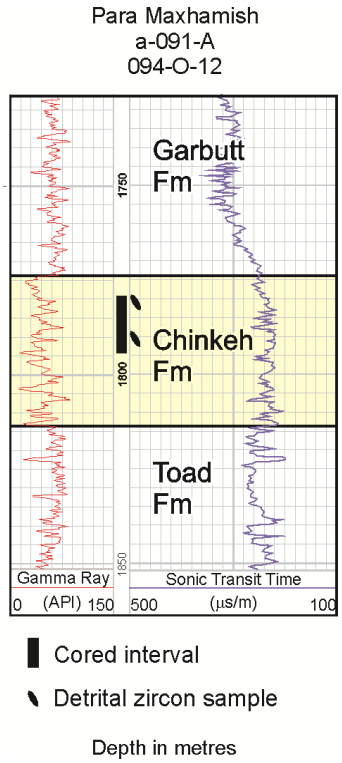

Figure 3. Location of samples collected from the Para Maxhamish Lake a-091-A/094-O-12 well. Core depths adjusted to reflect correlation of the core gamma ray trace with the borehole gamma ray signature.

DETRITAL ZIRCON METHODS

Sample Preparation

Samples were processed using a Bico™ Chipmunk crusher and pulverised using a Bico™ disc mill. The crushed material was pulverized to a final size of 350 µm. The pulverized sample was then run on an MD Gemini Goldharvester™ shaking table (water table) to reduce the volume of material by separating the intermediate and high density minerals (> 3.0 g/cm^3; including apatite, zircon, titanite, rutile) from low-density minerals (<3.0 g/cm^3; including quartz, micas, feldspars, calcite). The high and intermediate density fractions from the water table were combined, dried in an oven and sieved to remove material >1 mm. A hand magnet was used to remove metal filings introduced by processing the samples, and paramagnetic minerals such as magnetite and ilmenite. Bromoform (density 2.85 g/cm^3) was used to further concentrate the dense minerals.

Magnetic separation techniques can be used in U-Pb zircon-geochronology to increase analytical efficiency through the removal of grains likely to yield discordant analyses. The relationship between Pb-loss, discordance, and magnetic susceptibility was recognized by Silver (1963) and the procedure has since become an integral component of many U-Pb zircon studies. Sircombe and Stern (2002) investigated the possibility of introducing artificial bias in detrital zircon populations through the application of magnetic separation. Their results suggest that no significant bias in the measured detrital zircon populations was introduced and adequate analytical efficiency was achieved at a setting of 1.8A and 10° side-slope using a magnetic barrier separator. Magnetic barrier separators produce approximately >3.5 times higher magnetic flux density for a given current setting (S.G. Frantz Company Inc. documents) then isodynamic separators. We use a conservative maximum setting of 1.8A at 5° side-slope on an

isodynamic separator to minimize the likelihood of biasing the detrital zircon populations. No magnetic separation was undertaken on the core samples due to the small number of zircons recovered.

For the outcrop samples, a representative fraction was subsampled from the resulting zircon-rich mineral concentrate. The grain size distribution within the sample vial was homogenized by vigorous shaking, then between 1000 and 5000 zircons were selected using a scoop. To avoid biasing the analyzed detrital zircon population, no selection of grains according to their physical characteristics was undertaken. Due to the small size of the core samples all grains recovered from the sample were mounted. Grains were dumped into an alcohol-filled, 25.4 mm round plastic form epoxied to a Teflon sheet. The mounts were gently shaken to distribute the grains in a single layer and the alcohol was pipetted out of the form. The form was then allowed to dry completely and filled with Buehler EpoThin™, two-part epoxy and allowed to cure at room temperature for at least 24 hours prior to polishing.

Mounts were ground to expose the interior of the grains using 5 µm and 3 µm silicon carbide self-adhesive 3M polyester lapping films adhered to glass. Natural variability in grainsize within the detrital zircon population leads to some grains having a larger fraction of their diameter removed during grinding than others during grinding. Grinding of the mounts proceeded until the finest zircon population, in this study around 30 µm in diameter, was ground to no more than half its original thickness. As such, all zircon size populations within the mount were available for analysis and no grain-size bias was introduced. The final polishing step employed 1 µm diamond lapping film mounted on glass.

This method of mount preparation resulted in a very flat mount, little relief within the zircon crystals themselves (<<0.1 µm) and between the zircon and the surrounding epoxy (<0.3 µm; Figure 4). Approximately 1 µm of relief is present within the area of the mount analyzed. The flatness of the mount eliminates the possibility of isotopic ratios being affected by variation in laser focus at different locations on a grain (Marillo-Sialer et al. 2014) or within the grain mount, and allows for analyses to be placed very close to the edge of a grain or on small grains. Prior to ablation the samples were cleaned in an ultrasound using 18.2 MΩ water to reduce the effect of common lead on the surface of the sample.

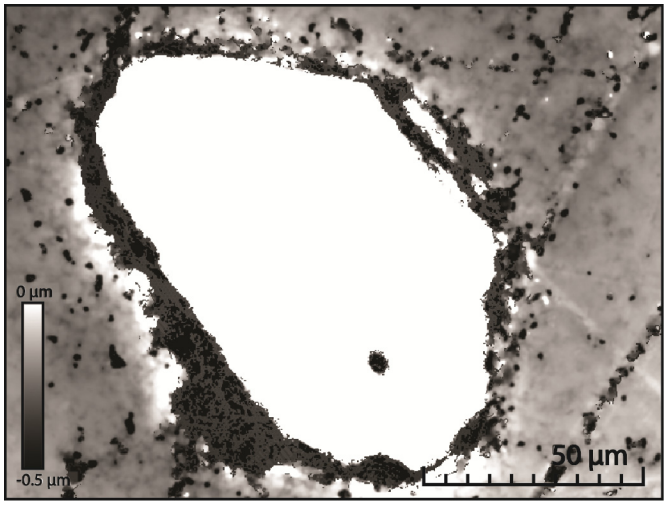

Figure 4. Optical profilometer image of the surface of a mount. The zircon shows no rounding toward the edges with <<0.1 µm of topography within the grain. The elevation of the grain above the surrounding epoxy is approximately 0.25 µm.

Analytical Procedure and Reduction

Uranium and lead isotopic ratios were measured by Laser Ablation Quadrupole Inductively Coupled Plasma Mass Spectrometer (LA-Q-ICP -MS) at the Center for Pure and Applied Tectonics and Thermochronology at the University of Calgary. A 20 or 30 µm beam diameter was chosen to fit ~95% of the zircons in the mount. To avoid biasing the detrital zircon population, ablation locations were chosen by systematically targeting every grain large enough to fit the chosen beam diameter and free of visible inclusions, fractures and alteration along a transect that spans the mount. This procedure eliminates grain-size bias and preserves the relative proportions of different age populations within the sample. Due to the small number of grains recovered from the core samples, all grains in these mounts were analyzed. Resolution of the laser optical microscope is sufficient to observe fractures that intersect the surface, and alteration and inclusions that appear as subtle variations in the intensity and texture of the reflected light.

Zircons were ablated in a Laurin Technic M-50™ dual-volume cell using an ASI Resochron™ 193 nm excimer laser ablation system. For a full description of the laser ablation system and characterization of the ablation cell see Muller et al. (2009). The very small inner ablation cell (volume of 1-2 cm^3) dramatically improves washout performance and reduces cell memory. A smoothing manifold (Squid) was used to smooth out the pulsed flow of analyte generated by the laser. Despite the use of a mixing manifold a decrease of approximately 5 orders of magnitude in signal intensity in ~3.5 seconds was achieved. A laser fluence of 1.5 J/cm^2 was employed and confirmed by measurement just above the ablation cell window with a Coherent Field Max II laser energy meter before each analytical session. A laser repetition rate of 7 Hz was used as it provided the optimum balance between signal intensity and pit depth. A 700 mL/minute flow of ultra-high (99.999%) purity He was employed to transport the ablated material from the ablation cell. Helium carrier gas maximizes sensitivity by minimizing redeposition of sample ejecta near the ablation site (Küper and Brannon, 1992; Horn and Günther, 2003). The carrier gas was combined with 750 mL/minute of argon and 6 mL/minute of N2 to increase sensitivity and reduce oxides (Durrant 1994, Guillong and Heinrich 2007) prior to introduction to the Q-ICP-MS.

Uranium and lead isotopic ratios were measured using an Agilent 7700 quadrupole Q-ICP-MS. Prior to each analytical session (typically 2 samples) the Q-ICP-MS was tuned for maximum sensitivity, minimum oxide production, and minimum uranium/thorium fractionation using NIST610 glass. Typical oxide production, measured using the 232Th/248ThO ratio, was less than 0.15% and the uranium/thorium ratio was within 1.5% of the known. Pulse-to-analogue tuning factors were calibrated before each run to ensure detector linearity. A list of measured isotopes and sample times per peak are given in Table 1.

Mercury is a common contaminant in LA-Q-ICP-MS gas systems and its presence can mask common lead derived from the ablation pit due to the isobaric interference of ^{204}Hg with ^{204}Pb. We use high-capacity Vici™ mercury traps on all gas supplies and monitor ^{201}Hg and ^{202}Hg during analysis. No correction for mercury interference was required in this dataset due very low background ^{201}Hg and ^{202}Hg.

Sixty-eight zircons were ablated from the upper core interval (1779.725-1779.78), 125 from the lower (1788.1-1788.2) and 140 grains from each of the outcrop locations along with ~15 primary and 20 ablations of 3 secondary references. References and unknowns were ablated under identical conditions. Each analysis began with a 15 second gas blank acquired with the laser off. This was followed by a 25 second ablation and a final delay of 5 seconds to record washout back to background levels. The rapid washout of the dual volume cell allowed approximately 12 s (43 sweeps) of data to be used to quantify backgrounds and 22 s (79 sweeps) to be used for each analysis.

The analytical sequence employed a reference-unknown bracketing procedure with primary references run every 10 unknowns (approximately 10 minutes). The well-characterized FC1 zircon (Paces and Miller, 1993) was used as the primary reference for characterizing and removing Laser Induced Elemental Fractionation (LIEF), calibrating the $^{206}Pb/^{238}U$ ratios, and correction for Instrumental Mass Fractionation (IMF). Zircon references Temora 2 (416.8; Black et al., 2004), 91500 (Weidenbeck et al. 1995) and GSC

internal reference 1242 (W.J. Davis, personal communication) were run as secondary references to assess the reproducibility and accuracy of the results. Background subtraction and correction for instrumental drift and mass fractionation (IMF), removal of laser induced elemental fractionation (LIEF) of U and Pb isotopes, calculation of uranium, thorium and lead concentrations, and determination of analytical uncertainties was performed in the Iolite™ software package (Paton et al. 2010) using the VisualAge data reduction scheme (Petrus and Kamber, 2012). All subsequent data manipulation and visualization was performed in Excel using the Isoplot plug-in (Ludwig, 2012).

Correction for Laser Induced Elemental Fractionation

Correction for LIEF is the most critical factor influencing the accuracy and precision of U-Pb age determinations by LA-Q-ICP-MS. Two methods are widely utilized by other labs. In the first method samples are corrected using a fractionation factor calculated from the average $^{206}Pb/^{238}U$ ratio determined from a corresponding time interval in the adjacent references (e.g., Van Achterberg et al. 2001; Jackson et al. 2004). In the second method a linear curve is fitted to the measured ratios and a y-intercept $^{206}Pb/^{238}U$ ratio is determined for the sample and the adjacent references (Sylvester and Ghaderi, 1997; Gehrels et al. 2008). The y-intercept $^{206}Pb/^{238}U$ ratio of the reference is then used to determine a fractionation factor for the sample. Because $^{206}Pb/^{238}U$ ratios are known to change, often in a non-linear fashion with increasing pit depth (Paton et al. 2010; Figure 5A), it is not possible by the intercept method to eliminate portions of an analysis compromised by lead-loss, common lead or inclusions without similarly modifying the time interval used to calculate the fractionation factor in the adjacent references.

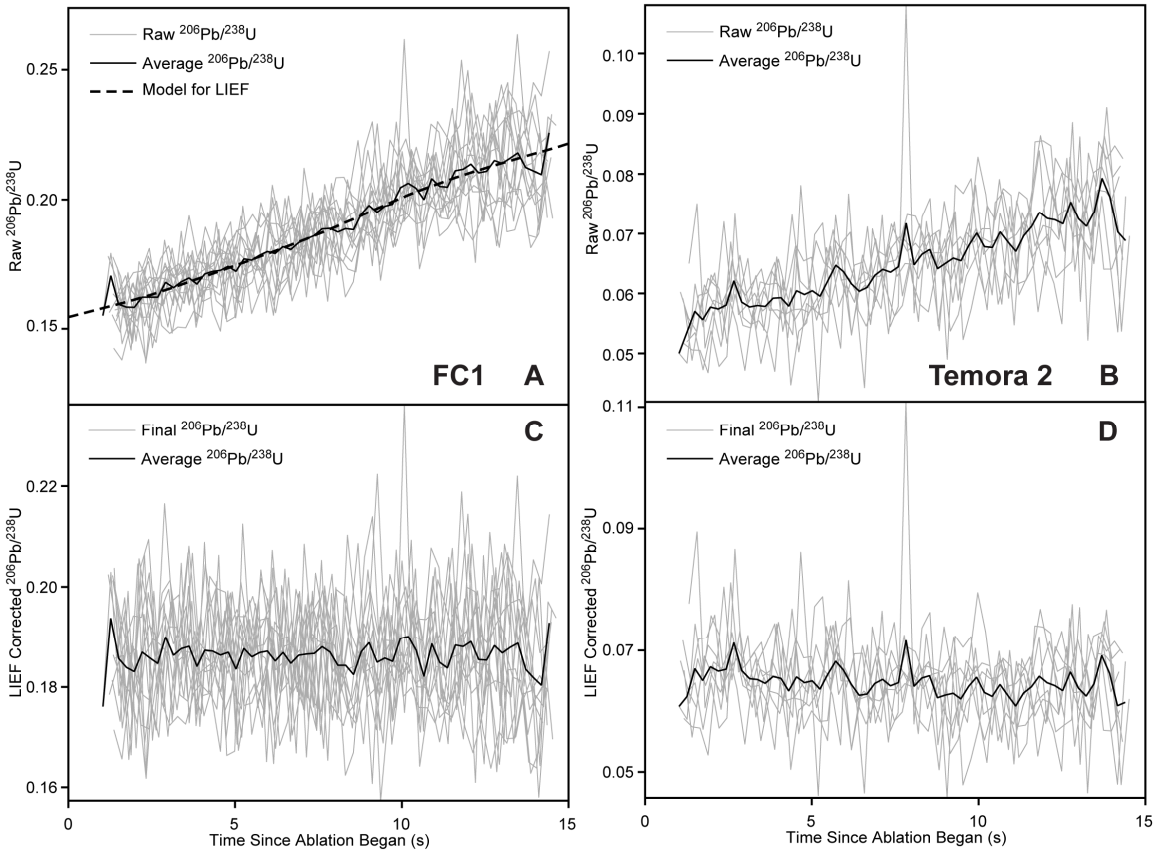

Figure 5. Raw (A, C) and LIEF-corrected $^{206}Pb/^{238}U$ ratios (B, D) for references FC1 and Temora 2.

To avoid this limitation, we follow the method outlined by Paton et al. (2010) and use the character of LIEF observed during ablations of the primary reference within the session to correct for it in the samples. For each session, the time-resolved, raw $^{206}Pb/^{238}U$ ratios from a minimum of 15 ablations of the primary reference (in this case FC1) were fitted using a smoothed cubic spline (Figure 5A) to define a model for LIEF in the analytical session. This model for the change in $^{206}Pb/^{238}U$ ratios with increasing pit depth is then used to correct for LIEF at each time-slice in the other analyses in the analytical session.

To illustrate the effectiveness of this method, raw and LIEF-corrected $^{206}Pb/^{238}U$ ratios for references FC1 and Temora 2 are shown in Figure 5. LIEF-corrected ratios for FC1 show no discernable systematic variability with time. A slight decrease in $^{206}Pb/^{238}U$ ratio in Temora 2 is likely caused by slight variations (1-2%) in the U and Pb fractionation behavior of the reference, related to differing crystallinities of Temora 2 and FC1 (Black et al. 2004; Marillo-Sialer et al. 2014; Matthews et al 2014).

A major advantage of this method for correcting LIEF is the preservation of temporal variation $^{206}Pb/^{238}U$ ratios during analysis (Paton et al. 2010). This temporal information combined with the fast washout of the M-50 cell allows for high vertical resolution within an analysis. In our apparatus vertical changes in isotopic ratios and trace-element concentrations of <2.5 μm can be resolved.

Calculation of Ages and Precision

Internal (or analytical) uncertainties are calculated in Iolite and are equal to the standard deviation of the $^{207}Pb/^{206}Pb$ and LIEF-corrected $^{206}Pb/^{238}U$ ratios (Paton et al. 2010). The mean ratios, internal uncertainties and error correlations for all analyses are exported from Iolite to Excel where the remainder of the uncertainty analysis and age calculations were undertaken in a custom spreadsheet. Analytical uncertainties are reported as the standard error of the mean (SEM) where n is the duration of the analysis in seconds.

The intra-sessional reproducibility of the isotopic ratios ($^{206}Pb/^{238}U$ and $^{207}Pb/^{206}Pb$) of secondary reference zircon 91500 (Weidenbeck et al. 1995) were used to assess whether additional, external, uncertainty was required in the session. Between 8 and 10 analyses of zircon 91500 were acquired in each session (~1 every 20 minutes). The weighted average of the $^{206}Pb/^{238}U$ and $^{207}Pb/^{206}Pb$ ratios were calculated and additional uncertainty required to make the secondary reference a single population (MSWD = 1) for each ratio was determined. This additional uncertainty was added quadratically to the analytical uncertainty for each analysis. A minimum external uncertainty of 1% was assessed on both ratios.

Ages were calculated using the Concordia age algorithm in the Excel plug- in Isoplot (Ludwig, 1998; Ludwig 2012). The Concordia age algorithm employs the $^{206}Pb/^{238}U$, $^{207}Pb/^{235}U$ and $^{207}Pb/^{206}Pb$ ratios and uncertainties, corrected for background, LIEF and IMF, to calculate an age, uncertainty and probability of concordance for each analysis. We utilize the quadratic sum of the analytical and external uncertainties in the Concordia age algorithm, as the combined uncertainty more realistically reflects the true precision of our measurement of these ratios.

Analytical precision improves with increasing age and uranium concentration (Figure 6). In general, higher uranium concentrations and older ages lead to higher ^{206}Pb and ^{207}Pb signal intensities and yield higher precision analyses. The uncertainty in the calculated Concordia ages varies systematically with age but is around 1.5% for analyses yielding Archean ages and increases to ~3% for analyses yielding ages in the late Mesozoic (2σ).

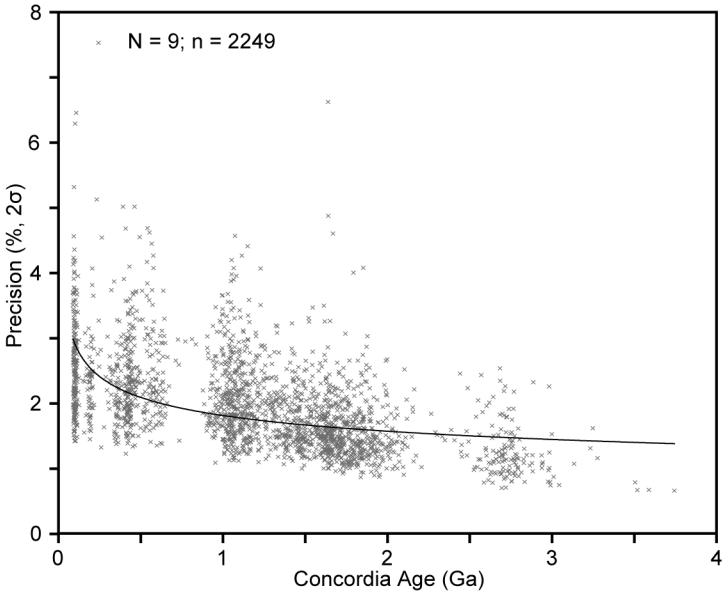

Figure 6. Precision of final Concordia age, including internal and reproducibility uncertainty, versus age for 9 analytical sessions including 2249 analyses. A best fit line (power curve) is fitted as a visual reference.

The calculation and reporting of Concordia ages yields a number of benefits. First, no arbitrary decision is required to choose the cutoff between $^{206}Pb/^{238}U$ and $^{207}Pb/^{206}Pb$ ages. Second, given the mean isotopic ratios and uncertainties, the Concordia age algorithm calculates the probability of concordance of the analysis, which can be used to filter the dataset (discussed below). Lastly, some improvement in precision is realized due to the integration of both measured isotopic ratios in the calculation of the age.

Data Filtering

Detection and elimination of spurious, or less reliable data, is an important step in U/Pb geochronology. Analyses may be compromised by a variety of geological and analytical factors such as lead loss during events subsequent to crystallization of the zircon, the intersection of fractures, inclusions and zones of alteration by the pit, and sampling different age domains within a zircon during a single analysis. Most of these factors lead to disturbance of the U/Pb isotopic system and result in discordant ages. As such, discordance filtering is the primary tool for eliminating less reliable data.

The discordance of a U/Pb analysis can be calculated as:

$$Discordance = \left(1 - \frac{^{206}Pb/_{^{238}U}Age}{^{207}Pb/_{^{206}Pb}Age}\right) x100$$

Analyses yielding positive discordance plot below the concordia curve while analyses yielding negative values plot above. Many data reduction methodologies apply discordance cutoffs, typically between +5% to +10% and -3% to -5%, to filter the data. The application of discordance filtering is complicated by the low precision of $^{207}Pb/^{206}Pb$ ratios measured in young grains (Phanerozoic), which leads to large variation in calculated $^{207}Pb/^{206}Pb$ ages and discordance. As such, discordance filters are

typically applied only to analyses older than ~500 Ma. Also, discordance filtering does not consider the precision of the individual analyses, only the calculated ages.

Concordia ages offer an attractive solution to these issues. The probability of concordance calculated by the Concordia age algorithm is a function of the precision of the measured ratios and the distance between the mean of the measurement (the center of the error ellipse) and the concordia curve. As such, high precision, moderately discordant ages (+5%), may yield a low probability of concordance and be eliminated from the dataset (Figure 7, A and B). Conversely, low precision, moderately discordant ages, may yield a relatively high probability of concordance and be accepted (Figure 7, C and D).

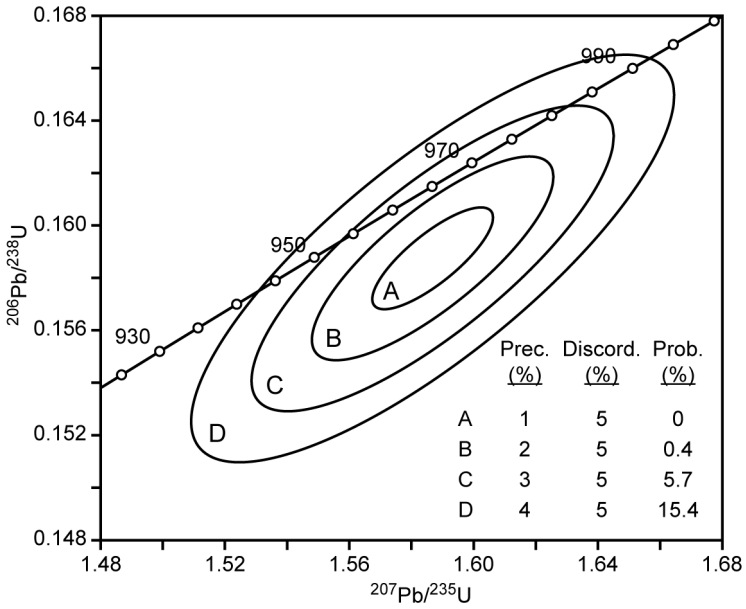

Figure 7. Error ellipses for a 5% discordant analysis at 1, 2, 3, and 4% precision. Higher precision analyses yield lower probabilities of concordance than lower precision analyses.

We eliminate analyses with a probability of concordance less than 1% from our dataset. To facilitate the comparison of our methodology to that employed by other labs we can empirically determine the approximate discordance cut-off in our dataset. The average, absolute discordance of all analyses >1 Ga, and the most discordant 200, that pass our criteria for concordance is 3.48% and 10.38%, respectively. Excluded data averages 10.59%.

The detection of mixed ages, where more than one age domain is sampled in a single ablation pit, presents unique challenges. Mixed ages will plot on a discordia connecting the ages of the two domains (Figure 5). If the age domains differ significantly in age (>1 Ga, Figure 8, A and B) the resulting analysis will be highly discordant (lying far from the concordia curve) for most proportional mixes of the two age domains and would be eliminated by discordance filtering. However, in cases where the two age domains are similar in age (Figure 8, C) mixed analyses will plot close to concordia and may, for typical analytical precisions, pass a discordance filter.

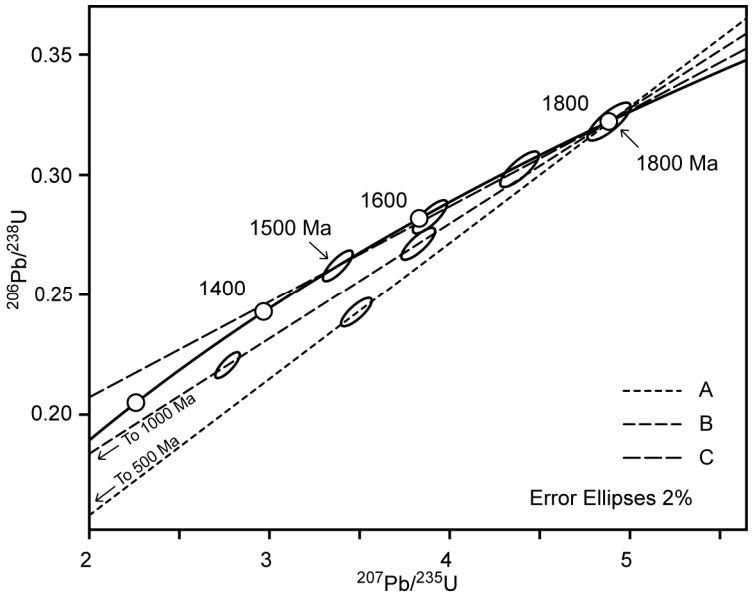

Figure 8. Concordia diagram showing analyses resulting from the mixing of two different age domains in a single analyses. A – 1800 Ma and 500 Ma; B – 1800 Ma and 1000 Ma; C – 1800 Ma and 1500.

Cathodoluminescence (CL) imaging is routinely employed in microanalytical methods to avoid choosing ablation locations that span two or more age domains. This practice originated in early ion microprobe work where it significantly improved the reliability of U/Pb zircon ages (Hanchar and Miller, 1993), and was adopted by the laser ablation community. However, CL imagery provides only two-dimensional constraint on the distribution of age domains in a zircon. While this geometric constraint is of little consequence to ion microprobe techniques, where ablation pits are <<1μm deep, it limits the usefulness of CL imagery in laser ablation, where pit depths are typically ~10 μm or more. As such, the information provided by CL imaging does not guarantee a homogenous age domain will be analyzed and a more holistic approach that integrates information in the depth domain, for the detection of mixed ages is required.

Rigorous interrogation of the $^{207}Pb/^{206}Pb$ and LIEF corrected $^{206}Pb/^{238}U$ ages, similar to commonly employed depth profiling techniques (e.g., Woodhead et al. 2004), can be used to detect age zonation, regions of lead loss and mixed ages that result from the laser sampling differing age domains (Jackson et al. 2004; Paton et al. 2010). Furthermore, integration of background-corrected signal intensities for uranium, thorium, zirconium and lead aid in the detection of inclusions, fractures and zones of alteration. Iolite provides an ideal environment for the detection of inhomogeneity as all of these parameters for a single ablation location can be rapidly and thoroughly scrutinized (Paton et al. 2010).

The orientation of the boundary between the two age domains is the primary control on the ability of this method to detect mixed ages. Age inhomogeneities are likely to be detected where the boundary between the age domains is oriented at a moderate to high angle to the ablation direction. This orientation provides maximum vertical and temporal resolution and in some cases both ages can be resolved in a single ablation. In cases where the boundary between the age domains is intersected at a low angle it may be more difficult to detect inhomogeneities as neither age will be well resolved. Similarly, a vertical boundary may be undetectable if the relative proportions of the two age domains being ablated is invariant during the analysis and the two age domains are of similar age. In this case it is possible that mixed ages may not be excluded from the final dataset. However, it is unlikely a grain population with complex age zonation would consistently present vertical boundaries and that the proportion of the two different age domains ablated at different locations would be similar. As such these special-case mixed ages would appear as single analyses between clusters of ages representing the two end-member age domains.

Inspection of time resolved age information above can also be used to improve the overall quality of the dataset by eliminating regions of lead-loss and portions of analyses contaminated by inclusions and common lead (Jackson et al. 2004).

Accuracy

The accuracy of the method was assessed by comparing the LA-Q-ICP-MS ages of secondary references from our study to their accepted ID-TIMS ages. Three secondary references, with ages from 416 Ma to 2679 Ma were analyzed. The weighted mean age for each reference was calculated for all analyses, in all analytical sessions in the dataset with no outlier rejection. All secondary references plot within 2% of their accepted ID-TIMS age and the absolute average offset is 1.35%.

REFERENCES

Black, L.P., Kamo, S.L., Allen, C.M., Davis, D.W., Aleinkoff, J.N., Valley, J.W., Mundil, R., Campbell, I.H., Korsch, R.J., Williams, I.S., and Foudoulis, C., 2003. Improved $^{206}Pb/^{238}U$ microprobe geochronology by the monitoring of trace-element-related matrix effects; SHRIMP, ID-TIMS, ELA-ICP-MS and oxygen isotope documentation for a series of zircon standards; Chem. Geol., vol. 205, p. 155-170.

Braman, D.R. and Hills, L.V., 1977. Source of Lower Cretaceous sandstone, Jackfish Gap, N.W.T.; Canadian Society of Petroleum Geologists (CSPG), Bulletin of Canadian Petroleum Geology, vol. 25, no. 3 (June), p. 631-634.

Durrant, S.F., 1994. Feasibility of improvement in analytical performance in laser ablation inductively coupled plasma-mass spectrometry (LA-ICP-MS) by addition of nitrogen to the argon plasma; J. Anal. Chem., vol. 349, p. 767-771.

Gehrels, G.E., Valencia, V.A., and Ruiz, J., 2008. Enhanced precision, accuracy, efficiency, and spatial resolution of U-Pb ages by laser ablation-multicollector-inductively coupled plasma-mass spectrometry; Geoch. Geoph. Geosys., vol. 9, p. 1-13.

Guillong, M. and Heinrich, C.A., 2007. Sensitivity enhancement in laser ablation ICP-MS using small amounts of hydrogen in the carrier gas; J. Anal. Atom. Spectr., vol. 22, p. 1488-1494.

Hanchar, J.M. and Miller, C.F., 1993. Zircon zonation patterns as revealed by Cathodoluminescence and backscattered electron images: Implications for interpretation of complex crustal histories; Chem. Geol., vol. 110, p. 1-13.

Horn, I., and Günther, D., 2003. The influence of ablation carrier gasses Ar, He, and Ne on the particle size distribution and transport efficiencies of laser-induced aerosols: implications for LA-ICP-MS; Appl. Surf. Sci., vol. 207, p. 144-157.

Jackson, S.E., Pearson, N.J., Griffin, W.L., and Belousova, E.A., 2004. The application of laser ablation-inductively coupled plasma-mass spectrometry to in situ U-Pb zircon geochronology; Chem. Geol., vol. 211, p. 47-69.

Jowett, D.M.S., 2004. Paleoenvironments and regional correlations of Albian-Cenomanian strata in the frontier Liard Basin of northwestern Canada; Ph.D. Thesis, Carleton University, Ottawa, Ontario, 419 p.

Küper, S. and Brannon, J., 1992. Ambient gas effects on debris formed during KrF laser ablation of polyimide; Appl. Phys. Lett., vol. 60, p. 1633-1635.

Leckie, D.A., Potocki, D.J., and Visser, K. 1991. The Lower Cretaceous Chinkeh Formation: a frontier-type play in the Liard Basin of Western Canada; American Association of Petroleum Geologists (AAPG), AAPG Bulletin, vol. 75, no. 3 (August), p. 1324-1352.

Ludwig, K.R., 1998. On the treatment of concordant Uranium-Lead ages; Geoch. Cosmoch. Acta, vol. 62, no. 4, p. 665-676.

Ludwig, K.R., 2012. Isoplot v. 3.75 – a geochronological toolkit for Microsoft Excel; Berkeley Geochronology Center, Special Publication, no. 5, p. 1-75.

Marillo-Sialer, E., Woodhead, J., Hergt, J., Greig, A., Guillong, M., Gleadow, A., Evans, N., and Paton, C., 2014. The zircon 'matrix effect': evidence for an ablation rate control on the accuracy of U-Pb age determinations by LA-ICP-MS; J. Anal. Atom. Spectr., vol. 29, p. 981-989.

McMechan, M., Currie, L., Matthews, W., Ferri, F., and Guest, B., 2015. Detrital zircon geochronology and the evolution of clastic source areas, Liard Basin, northeast British Columbia. Geoconvention 2015, abstract. <http://www.geoconvention.com/archives/2015/250_GC2015_Detrital_zircon_geochronology.pdf> [accessed April 11, 2016].

McMechan, M., Matthews, W., Ferri, F., and Guest, B., in press. Maximum age of the basal Cretaceous Chinkeh Formation sandstones, Maxhamish Lake area, Liard Basin, British Columbia; Bulletin of Canadian Petroleum Geology, vol. 64, no.3.

Müller, W., Shelley, M., Miller, P., and Broude, S., 2009. Initial performance metrics of a new custom-designed AfF Excimer LA-ICPMS system coupled to a two-volume laser-ablation cell; J. Analy. Atom. Spectr., vol. 24, p. 209-214.

Paces, J.B. and Miller, J.D., 1993. Precise U-Pb ages of Duluth Complex and related mafic intrusion, Northeastern Minnesota: Geochronological insights to physical, petrogenetic, paleomagnetic, and tectonomagmatic processes associated with the 1.1 Ga Midcontinent Rift System; J. Geoph. R., vol. 98, p. 13997-14013.

Paton, C., Woodhead, J.D., Hellstrom, J.C., Hergt, J.M., Greig, A., and Maas, R., 2010. Improved laser ablation U-Pb zircon geochronology through robust downhole fractionation correction; Geoch. Geoph. Geos., vol. 11, p. 1-36.

Petrus, J.A. and Kamber, B.S., 2012. VizualAge: A novel approach to laser ablation ICP-MS U-Pb geochronology data reduction; Geost. and Geoanal. R., vol. 36, no. 3, p. 247-270.

Silver, L. and Deutsch, S., 1963. Uranium-lead isotopic variations in zircon: a case study; J. Geol., vol. 71, p. 721-758.

Sircombe, K.N. and Stern, R.A., 2002. An investigation of artificial biasing in detrital zircon U-Pb geochronology due to magnetic separation in sample preparation; Geoch. Cosmoch. Acta., vol. 66, no. 13, p. 2379-2397.

Sylvester, P.J. and Ghaderi, M., 1997. Trace element analysis of scheelite by excimer laser ablation-inductively couple plasma-mass spectrometry (ELA-ICP-MS) using a synthetic silicate glass standard; Chem. Geol., vol. 141, p. 49-65.

Van Achterbergh, E., Ryan, C.G., Jackson, S.E., and Griffin, W.L., 2001. Data reduction software for LA-ICP-MS: appendix; *in* Sylvester, P.J. (Ed.), Laser Ablation-ICP-Mass Spectrometry in the Earth Sciences: Principles and Applications; Mineralog. Assoc. Canada (MAC) Short Course Series, Ottawa, Ontario, Canada, vol. 29, p. 239-243.

Woodhead, J., Hergt, J., Shelley, M., Eggins, S., and Kemp, R., 2004. Zircon Hf-isotope analysis with an excimer laser, depth profiling, ablation of complex geometries, and concomitant age estimation; Chem. Geol., vol. 209, p. 121-135.

Weidenbeck, M., Alle, P., Corfu, F., Griffin, W.L. Meier, M., Oberli, F., Von Quadt, A., Roddick, J.C., and Spiegel, W., 1995. Three natural zircon standards for U-Th-Pb, Lu-Hf, trace element and REE analysis; Geost. Newsl., vol. 19, no. 1, p. 1-23.

LIST OF FIGURES

LIST OF TABLES